

# Ursolic Acid Loaded Transniosomes Nanogel for Topical Delivery: Statistical Optimization with Box-Behnken Design of Quality by Design (QbD), *in vitro* and Dermatokinetic Evaluation

Hafiz A. Makeen<sup>1,\*</sup>, Mohammad Albratty<sup>2</sup>

<sup>1</sup>Pharmacy Practice Research Unit, Department of Clinical Pharmacy, College of Pharmacy, Jazan University, Jazan, SAUDI ARABIA.

<sup>2</sup>Department of Pharmaceutical Chemistry and Pharmacognosy, Faculty of Pharmacy, Jazan University, Jazan, SAUDI ARABIA.

## ABSTRACT

**Aim:** The current research was performed for the preparation and optimization of Transniosomes (TN) preparation for the dermic distribution of Ursolic Acid (UA). **Materials and Methods:** The formulation was optimized by using the "Box-Behnken design" software. Particles size, % EE, and *in vitro* study was performed for the optimal formulations after they had been optimised. In addition, morphological, CLSM and dermatocokinetic studies were performed in order to complete the evaluation of the optimal formulation of TN. **Results:** The improved UA-TN formulation showed vesicles in the shape of lamellae that were completely sealed, with particles size, percentage EE and *in vitro* release of  $145.5 \pm 2.56$  nm,  $84.74 \pm 2.49\%$  and  $86.28 \pm 1.74\%$  respectively. The percentage cumulative drug permeated through skin for UA-CF gel and UA-TN gel was 36.30% and 84.05% respectively. When equated to the Rhodamine B-hydro methanolic liquid, the confocal pictures that were acquired of rat skin evidently demonstrated that the loaded rhodamine B with TN gel formulation allowed for a deeper penetration of the substance. Further, the UA-TN gel applied mice skin disclosed significant changes in  $C_{\text{Skin max}}$  and  $AUC_{0-8}$  in compare to rat skin applied with UA-CF gel formulation. **Conclusion:** The successful optimization and characterization of TN of UA using Box-Behnken design and enhanced dermal delivery reflect the novelty of the work. Present research data showed that the developed TN vesicle formulation was found to be effectively useful drug carrier for UA topical delivery.

**Keywords:** Ursolic acid, Dermal, Confocal laser scanning microscopy, Dermatokinetic, Skin cancer, Transniosomes, Tumors.

## Correspondence:

**Hafiz A. Makeen**

Pharmacy Practice Research Unit,  
Department of Clinical Pharmacy, College  
of Pharmacy, Jazan University, Jazan,  
SAUDI ARABIA.  
Email: hafiz@jazanu.edu.sa

**Received:** 17-03-2023;

**Revised:** 16-07-2023;

**Accepted:** 14-08-2023.

## INTRODUCTION

Skin cancer is on the rise and has become a silent killer. It is one of the most prevalent cancers in the globe. In recent years, the diagnosis has expanded drastically in several nations. The United States has a high incidence of Non-Melanoma Skin Cancer (NMSC), which accounts for about 5.4 million treatments yearly.<sup>1</sup> The incidence of NMSC surpasses 2,000 per 100,000 person-years in Australia.<sup>2</sup> The Australian cancer registry research documents an incidence of more than 12,000 basal cell carcinomas per 100,000 person-years in those older than 80.<sup>3</sup> In addition to melanoma, the most often diagnosed NMSCs include basal cell carcinoma and squamous cell carcinoma.<sup>4</sup> Squamous cell

carcinoma is regarded as the most malignant due to its aggressive character, which can result in metastasis and mortality.<sup>5</sup> For the management of skin disorders and infections, the dermic pathway of medication delivery has been one of the most recommended ways. The dermal approach has garnered considerable interest in recent years.

Triterpenoids, a large family of natural chemicals with more than 20,000 members in the plant kingdom, are one of the most diverse chemical classes.<sup>6,7</sup> As revealed by clinical and preclinical research,<sup>8,9</sup> pentacyclic triterpenes constitute a separate class of triterpenoid natural compounds with unique biological activities. As a hydroxy pentacyclic triterpene acid, ursolic acid (3b-hydroxy-12-urs-12-ene-28-oic acid) is commonly found in medicinal plants and is a component of the waxy coats on a variety of fruit species, such as apples, pears, olives, prunes, and cranberries. Water solubility is low and inability to permeate few biological membranes, the BCS classification categorised UA as a class IV medication with minimal pharmacological



DOI: 10.5530/ijper.58.1.11

### Copyright Information :

Copyright Author (s) 2024 Distributed under  
Creative Commons CC-BY 4.0

Publishing Partner : EManuscript Tech. [www.emanuscript.in]

action. Poor oral bioavailability of the drugs in this class<sup>10,11</sup> is the result of their sluggish dissolving and limited gastrointestinal mucosa penetration. Ursolic Acid (UA) is a potent medicine with several therapeutic qualities, including hepatoprotection,<sup>12,13</sup> immunomodulation,<sup>14</sup> anti-inflammatory,<sup>15,16</sup> anti-diabetic,<sup>17</sup> anti-bacterial,<sup>18,19</sup> anti-viral,<sup>20,21</sup> anti-ulcer,<sup>22</sup> and anti-cancer activity.<sup>23</sup> Recent investigations have shown that UA possesses multifunctional anticancer activities.<sup>23,24</sup> As a dietary component, UA is also linked in the prevention and treatment of cancer.<sup>25,26</sup> In the context of cancer therapy, UA interrelates with a variety of molecular targets that play a crucial part in several cell signalling cascades. It inhibits tumour cell transformation and proliferation and promotes apoptosis. The limited therapeutic uses of ursolic acid in clinical medication are due to its low bioavailability and absorption of drug. The anticancer benefits of UA can be associated to its capability to induce apoptosis in cancer cell, prevent tumour formation, and decrease cancer cell proliferation, according to an accumulation of mechanistic research. Several signalling pathways, such as NF- $\kappa$ B,<sup>27</sup> STAT3,<sup>28,29</sup> and TRAIL,<sup>30</sup> induce cancer cell autophagy, cell cycle arrest, and apoptosis.<sup>23</sup> UA disrupts the NF- $\kappa$ B pathway by blocking the phosphorylation of p65, resulting in the downregulation of numerous downstream oncogenes, including Bcl-2 and Bcl-XL.<sup>23</sup> However, the precise molecular pathways by which UA causes apoptosis and reduces cancer growth have yet to be determined.<sup>23</sup> Signaling pathways may be altered progressively or concurrently and may interact synergistically in several cancer cell types to aid UA treatment.<sup>31</sup> Although UA demonstrated substantial safety and effectiveness when used to treat cancer, its low solubility, quick metabolism, and poor bioavailability hampered its therapeutic potential and clinical uses.<sup>32</sup>

In the present work, cutaneous administration of UA was improved utilising Box-Behnken design. The TN possessed both niosome and transfersome benefits. Since TN vesicles included edge activators, they demonstrated improved penetrability and deposition, as well as enhanced drug stability, solubility, and permeation. Consequently, A TN formulation that, in addition to phospholipids, also included non-ionic surfactant and edge activators demonstrated the beneficial properties of both niosomes and transfersomes. Since TN had both edge activator and non-ionic surfactant, it was more successful at penetrating the skin than niosomes, which only contained non-ionic surfactant. The addition of TN into gel might potentially increase formulation viscosity and, consequently, duration of time that the formulation is present at the application location.<sup>33</sup>

The purpose of this study was to design and optimise UA-TN by altering independent factors such as Lipoid S100, Span 60, and Cholesterol content. The impact of the dependent variables particles size, % EE, and *in vitro* release was analysed by using Box Behnken Design (BBD). In addition, the optimal UA preparation

was examined for vesicle shape, skin permeation and penetration properties, antioxidant activity, and Dermatokinetic studies.

## MATERIALS AND METHODS

Ursolic acid, Lipoid S100, cholesterol, triethanolamine, sodium cholate, gelling agent, surfactant, and co-surfactant (Span60 and PEG 400) were purchased from Sigma-Aldrich (USA). Carbopol 980 was procured from SD fine chemicals. All the chemicals and solvents used in the tests were analytical grade, and HPLC-grade water was used throughout the procedure.

### Development of UA-TN formulation

Lipoid S100, Cholesterol, Span 60, and UA were combined in methanol for the production of TN of UA. In the flask, a film is deposited by the rotary evaporator in the form of a very thin layer under reduced pressure by creating a vacuum and removing the organic solvent. The dried thin layer was rehydrated using pH 7.4 solution containing sodium cholate for 1 hr at room temperature while rotating at 120 revolutions per minute. For size reduction, the generated dispersions were then probe-sonicated for 4 min. Based on vesicle size, % EE, cumulative *in vitro* release, and morphological characteristics, the TN were characterised. BBD with 3 factor and 3 levels was used in design expert and the chosen variables are shown in Table 1.

### BBD Statistical

Various factors, such as the quantity of Lipoid S100, Cholesterol, and Span 60, play main roles in the efficacious preparation of UA-TN. These factors affect particle size, % EE, and *in vitro* drug release. One of the most important roles that these factors play is in the successful development of UA-TN. Therefore, in the current experiment, the concentrations of Lipoid S100, Cholesterol, and Span 60 were adjusted by BBD with the use of DOE software (Design-Expert, v-12, Minnesota, United States) in order to facilitate the effective creation of UA-TN. As shown in Table 1, the concentrations of Lipoid S100 ( $X_1$ ), Cholesterol ( $X_2$ ), and Span 60 ( $X_3$ ) were chosen as independent factors for the purpose of optimising UA-TN by BBD. These concentrations were each selected at three different levels: high (coded as "+1"), medium (coded as "0"), and low (coded as "-1"), respectively. The three-factor, three-level BBD was used to optimise the formulation of UA-TN. According to the design software, seventeen UA-TN formulations (Table 2) were generated and assessed. On the other hand, the responses were thought to be the vesicle size of the UA-TN (which was coded as  $R_1$ ), the entrapment effectiveness of the UA-TN (which was coded as  $R_2$ ), and the cumulative *in vitro* drug release (which was coded as  $R_3$ ).

### TN particles size and Polydispersity Index (PDI)

A zeta sizer was utilised in order to conduct research on the particles size, PDI, and Zeta Potential (ZP) of UA-TN. After putting the materials into the zeta cuvette, the experiment was

**Table 1: BBD independent and dependent variables for the preparation and optimization of UA-TN.**

Variables	Used Levels		
	Low (-1)	Medium (0)	High (+1)
Independent variables			
X <sub>1</sub> = Lipoid S100 (mg)	60	80	100
X <sub>2</sub> = Span 60 (mg)	15	20	25
X <sub>3</sub> = Cholesterol (mg)	10	15	20
Dependent variables			
Y <sub>1</sub> = Particles size (nm)	Minimum		
Y <sub>2</sub> = EE (%)	Maximum		
Y <sub>3</sub> = <i>In vitro</i> release (%)	Maximum		

**Table 2: Observed responses for the optimization of UA-TN formulation and summary of results of regression analysis for responses Y<sub>1</sub>, Y<sub>2</sub> and Y<sub>3</sub> for fitting to quadratic model.**

Formulations	Independent variables			Dependent variables		
	X <sub>1</sub>	X <sub>2</sub>	X <sub>3</sub>	Y <sub>1</sub>	Y <sub>2</sub>	Y <sub>3</sub>
1	80	25	20	150.94 ± 2.16	80.79 ± 2.75	69.64 ± 1.48
2	100	20	20	165.37 ± 1.05	74.94 ± 1.49	63.68 ± 2.44
3	80	20	15	147.24 ± 2.42	84.11 ± 1.09	84.98 ± 3.72
4	80	15	10	159.01 ± 3.05	77.67 ± 2.85	59.84 ± 2.95
5	80	20	15	145.50 ± 2.56	84.74 ± 2.49	86.28 ± 1.74
6	100	15	15	192.58 ± 1.95	73.27 ± 2.46	58.84 ± 2.38
7	100	20	10	171.16 ± 3.59	77.84 ± 1.48	65.68 ± 3.94
8	60	15	15	188.86 ± 2.95	58.84 ± 2.47	64.99 ± 2.45
9	80	15	20	160.34 ± 1.44	76.87 ± 3.85	61.72 ± 3.05
10	80	25	10	153.04 ± 2.34	82.59 ± 1.74	66.27 ± 4.02
11	100	25	15	182.12 ± 3.68	76.37 ± 3.49	60.18 ± 2.04
12	60	20	20	158.12 ± 2.48	65.39 ± 2.48	73.57 ± 2.38
13	60	25	15	174.01 ± 3.12	64.23 ± 1.49	68.94 ± 2.48
14	80	20	15	149.17 ± 2.43	82.78 ± 3.18	84.37 ± 2.04
15	80	20	15	147.53 ± 2.49	83.58 ± 2.46	86.01 ± 2.18
16	60	20	10	168.95 ± 1.58	69.73 ± 2.53	70.39 ± 2.19
17	80	20	15	148.17 ± 3.69	83.22 ± 1.38	85.14 ± 3.01
Quadratic model	R <sup>2</sup>	Adjusted R <sup>2</sup>	Predicted R <sup>2</sup>	SD	%CV	Mean
Response (Y <sub>1</sub> )	0.9857	0.9674	0.8009	2.72	1.67	162.48
Response (Y <sub>2</sub> )	0.9845	0.9645	0.7864	1.46	1.92	76.29
Response (Y <sub>3</sub> )	0.9911	0.9797	0.8788	1.45	2.04	71.21

X<sub>1</sub> = Lipoid S100 (mg), X<sub>2</sub> = Cholesterol (mg), X<sub>3</sub> = Sodium cholate (mg), Y<sub>1</sub> = Vesicles size (nm), Y<sub>2</sub> = Entrapment efficient (%) and Y<sub>3</sub> = *in vitro* release (%).

performed out at room temperature with a scattering angle of 90°. The preparation was dispersed in buffer solution of pH 7.4 for the investigation, and measurements were conducted thrice.

**Transmission Electron Microscopic (TEM) Analysis**

Under a transmission electron microscope, the structure of the improved UA-TN was analysed for its morphology (TEM;

Morgagni 268D, Eindhoven, The Netherlands). In order to achieve point-to-point resolution using the microscope, the operating voltage was set to 200 kV. On a copper grid of 300 mesh, a drop of UA-TN was placed, and then the grid was stained negatively with 1% phosphotungstic acid. Following this step, the grid was allowed to air dry before being seen using a microscope.<sup>34,35</sup>

## Entrapment efficiency (%EE)

An indirect technique that utilised centrifugation was utilised in order to determine the %EE and %LC of UA-TN [20]. In a nutshell, UA-TN were centrifuged for 15 min at fifteen thousand revolutions per minute with the assistance of a cooling centrifuge. Following this, the upper layer was removed and passed through 0.2 µm filter.<sup>36</sup> After that, the amount of untrapped UA was quantified with the assistance of a UV-Spectroscopy (model UV-1601) set to a maximum wavelength of 215 nm.<sup>37</sup> The below formula was utilised in order to compute the % EE and % LC.

$$\%EE = \frac{(Total\ weight\ UA - UA\ in\ supernatant)}{Total\ weight\ UA} \times 100$$

$$\%LC = \frac{(Total\ weight\ UA - UA\ in\ supernatant)}{Total\ weight\ TN} \times 100$$

## In vitro study

The dialysis bag technique was utilised in order to determine the amount of UA that was released *in vitro* from the optimised UA-TN and UA suspension (UA-CF).<sup>38</sup> Prior to carrying out the study, the dialysis bag was prepared for use by activating it in accordance with the protocol recommended by Sigma Aldrich. Following this step, about 2.5 mL of UA-TN solution was taken in a dialysis bag, and then thread was used to tie both ends of the bag. After that, the preparation, which included the bag, was submerged in the medium for dissolving (500 mL). The study was performed at temperature  $32 \pm 1^\circ\text{C}$ , with a continuous stirring at 100 revolutions per minute. Aliquots of 3 mL were obtained at predetermined intervals, and an equivalent volume of fresh medium was replaced at regular intervals in order to keep the sink state constant. The extracted material was filtered, then adequately diluted, and the amount of UA that was released was calculated by evaluating the absorbance of UA using a UV-Spectroscopy at 215 nm.<sup>37,39</sup> The release of UA was assessed using a process that was quite similar, and the findings were compared in order to assess the dissolution enhancing capacity of the optimised UA-TN. The *in vitro* release data were used to study the kinetics of UA release from the improved UA-TN by fitting them into a number of different mathematical models. In order to investigate the process by which UA is released from the optimised UA-TN, the model that produced the maximum R<sup>2</sup> value was deemed to be the model that provided the most accurate representation of the data.<sup>40</sup> Various mathematical models were used to predict the *in vitro* drug release data from a dose form.<sup>41</sup>

## Antioxidant activity

### DPPH Assay

This test was utilised in order to evaluate the antioxidant capacity of the improved UA-TN, and free UA was assessed in

accordance with the described procedure, but with some minor adjustments.<sup>42</sup> In order to carry out this experiment, both free UA and the optimised UA-TN were first dissolved in ethanol to produce stock solutions with a concentration of 10 mg/mL. After diluting the stock solutions, a series of dilutions between 20 to 100 µg/mL was done in the lab. After obtaining the solution, it was filtered using a membrane filter with a 0.4-micron pore size in order to eliminate any residue that could have been present in the solution. Then a solution of 0.02% DPPH in ethanol was made, and 0.5 mL of each solution of free UA was added to that solution. Finally, the optimised solution was added to 125 µL of the DPPH solution. In order to finish the reaction, the mixture that was produced was given a light vortexing and then stored in a dimly lit area for an hour. The conclusion of the reaction may be identified by the absence of any colour in the solution, which had previously been violet. Using a UV spectrophotometer, a reading of 517 nm was obtained for the absorbance after 1 hr had passed. A high value for the sample's radical scavenging potential is correlated with a low absorbance value. In addition, a process very identical to that which was followed, but this time DPPH solution was used as the control, and the values were related. At end, the percentage of RSA, was determined with the assistance of the following eq. Following is the formula that was utilised in the calculation of the antioxidant activity %.<sup>33</sup>

$$\%RSA_{DPPH} = \frac{(\text{Abs. of control} - \text{Abs. of the sample})}{\text{Abs. of control}} \times 100$$

### ABTS Assay

This test was utilised in order to test the antioxidant capacity of the improved UA-TN, and free UA was analysed in accordance with the described procedure, but with some slight adjustments.<sup>43</sup> In order to carry out this experiment, both free UA and the optimised UA-TN were first dissolved in ethanol to produce stock solutions with a concentration of 10 mg/mL. After diluting the stock solutions, a series of dilutions between 20 to 100 µg/mL was done in a lab. After obtaining the solution, it was filtered using a membrane filter with a 0.4-micron pore size in order to eliminate any residue that could have been available in the solution. Then, 0.1 mL of the sample was added at each solution to 0.9 mL of the ABTS solution. This process was repeated three times. In order to finish the reaction, the mixture that was produced was placed in a dimly lit area on top of a water bath and left there at room temperature for 30 min. After 30 min, a UV-spectrophotometer showed that the absorption had reached 734 nanometers. In addition, the ABTS solution was used as a control in a technique that was quite similar to the original one, and then the results were compared. After everything was said and done, the %RSA was computed with the aid of equation.<sup>36</sup>

$$\%RSA_{ABTS} = \frac{(\text{Abs. of control} - \text{Abs. of the sample})}{\text{Abs. of control}} \times 100$$

### Preparation of UA-TN gel

For the TN formulation to remain on the skin of mice for an extended amount of duration, it must be sufficiently viscous. The produced UA-TN was therefore put into a gel composition. To produce gel, a measured quantity of Carbomer 980 with a weight-to-volume ratio of 1% was added to double-distilled water and stirred until a uniform dispersion was obtained. The mixed solution was left overnight to fully expand. As preservatives, PEG 400 (15%) and 0.1% of chlorocresol was transferred to the mixture afterwards. Triethanolamine was added as a pH-adjusting agent to the mixture. On the basis of continual agitation, the optimised UA-TN was then taken dropwise to this preformed gel to get a homogenous gel formulation.<sup>44,45</sup>

### Determination of pH and texture of UA-TN gel

1 g of UA-TN gel formulation was dissolved in double-distilled water. Wait 1 min for equilibrium before measuring the pH with a digital pH metre electrode. In addition, for gel, the programme TA.XT Plus Texture Analyzer was utilised. To prevent the formation of air bubbles, 50g of each manufactured gel formulation (blank gel and optimised UA-TN gel) was taken in a 100 mL glass container and test according to the normal protocol outlined in our earlier papers.<sup>33,46</sup> The final result is a texture analysis curve that reveals the gel properties.

### Extrudability

A clamp was put on the crimped end of a closed collapsible tube with about 20 gm of gel inside to keep it from rolling back. Once the cap was taken off, the gel came out. The quantity of gel that came out of the hole was collected and weighed. The amount of gel that was pushed out was figured out.<sup>47</sup>

### Spreadability

Standard-sized glass slides were used to create two sets of images. One of the slides had the enhanced topical gel composition applied to it. The gel was then placed on top of a second slide, creating a 7.50 cm long sandwich. There was a thin layer of gel created by spreading 100g of gel on the top slides and pressing them together. The surplus of gel that had attached to the slides was also removed, as was the weight. The two slides were attached to the platform in such a way as to cause little disturbance, and the weight attached to the top slide limited its motion to the vertical plane. The top slide was fitted with a 20g weight. The time it took for the top slide to move the 7.50 cm and disengage from the bottom slide under the force of the weight was measured.<sup>47</sup>

### Stability testing for the gel preparation

The fundamental goal of stability study is to learn how the drug's superiority changes with time as a consequence of environmental conditions like temperature and humidity. This topical gel formulation underwent a stability study in a stability chamber for a full six months, as per ICH guidelines. A humidity chamber

was set up with temperature  $25^{\circ}\text{C} \pm 2^{\circ}\text{C}$ ,  $32^{\circ}\text{C} \pm 2^{\circ}\text{C}$  and  $40^{\circ}\text{C} \pm 2^{\circ}\text{C}$  with RH  $60\% \pm 5\%$ ,  $60\% \pm 5\%$  and  $75\% \pm 5\%$  RH respectively for UA-TN. Changes in colour, odour, homogeneity, pH, and viscosity were measured from the initial sample to subsequent samples taken at 1, 2, 3, and 6 months.<sup>47</sup>

### Skin permeation study

Franz diffusion cell was used, which was having surface area of  $0.785\text{ cm}^2$  for the purpose of diffusion were used to conduct skin permeation experiments. The donor compartment was non-occlusively accessed, and 1 g of the UA-TN gel formulation was removed. For the duration of the experiment, the saline (pH 7.4) solution receiver vehicle (10 mL) was agitated at 600 rpm and held at  $37 \pm 1^{\circ}\text{C}$  [33]. At regular intervals, 1 mL samples were taken from the bottom (receiver) compartment (0, 1, 2, 4, 6, 8, 12 and 24 hr). The withdrawn sample was substituted instantly with a same mL of new saline solution. Each sample was analysed by the HPLC technique to determine its UA concentration. The UA was calculated to be at a 215 nm wavelength.<sup>33</sup>

### Determination of depth of skin penetration

Confocal Laser Scanning Microscopy (CLSM) was employed to characterise the tissue uptake analysis of the rhodamine B-loaded UA-TN gel and the rhodamine B-hydro methanolic solution. The skin of mice was glued on two distinct Franz diffusion cells, treated with UA-TN, and then a hydro methanolic solution loaded with rhodamine B dye was applied in a homogeneous and non-occlusive manner. The cells were then set aside for 8 hr at  $37^{\circ}\text{C}$ . Following the completion of the experiment, both skins were given a wash in double-distilled water to rid them of any surplus formulations or hydro methanolic solution, and then they were then sliced up into little section for the preparation of glass slide. After positioning the set slides such that the stratum corneum was facing skyward, the data was collected using a CLSM. The Z-axis was used to perform the scanning, and the increments used were  $5\text{ }\mu\text{m}$ . In order to excite the fluorescence, an argon laser beam of wavelength 488 nm was employed, and a wavelength of 532 nm was utilised for the measurement of the fluorescence emission. The Leica Application suite Advance Fluorescence software was utilised in the process of carrying out the depth measurements.<sup>33</sup>

### Dermatokinetic study

A dermatokinetic research was carried out on mice in order to ascertain the amount of medication that was present in both the epidermis and the dermis layers of their skin. The skin of mice was put on a Franz diffusion cell for the purpose of the study. UA-TN gel preparation was then used on the skin, and the examination was performed in the same manner as was described under the *in vitro* skin permeation study heading. As per the investigation, the used skin of mice was withdrawn from the Franz diffusion cell at regular time intervals such as 0, 1, 2, 4, and 8 hr.<sup>48</sup> The equipment

was disassembled, and the skin was cleansed with regular saline before being placed in water for two to 3 min at a temperature of 60°C. After that, the layers of skin are peeled back using forceps, and then they are cut into smaller and smaller bits. After that, the fragments are submerged in 5 mL of methanol for 24 hr in order to extract UA. Following this step, the methanolic extract of UA was filtered through a membrane, and the HPLC technique was used to determine the amount of UA present in the sample.<sup>49</sup> The UA concentrations per cm square of skin were plotted against the passage of time on a graph, with each layer represented by its own unique line. In order to conduct an analysis of the various dermatokinetic parameters, such as  $T_{\text{skin max}}$  and  $C_{\text{skin max}}$  as well as  $AUC_{0-8h}$  and  $K_e$ , the PK solver programme was used.

## RESULTS AND DISCUSSION

### Optimization of UA-TN by BBD

The result was obtained after the preparation of 17 formulations, and the value of each response, namely  $R^1$ ,  $R^2$ , and  $R^3$ , was fitted in 3 different models using the software. The value of each response was then analysed using linear regression to determine which model was the best fit. The statistical model that produced an adjusted and anticipated  $R^2$  that was closest to one was chosen as the model that best suited the data because it produced the greatest adjusted  $R^2$  (Table 2). If the value of "p" for the model's terms is  $< 0.05$ , then the model is regarded to contain statistically significant terms. According to the findings, which are presented in Table 2 and are summarised there, the quadratic model was selected as the good-fitting statistical model since it has the greatest adjusted and anticipated  $R^2$  for all three levels. The following is the quadratic polynomial equation that was derived by using the Design Expert® programme for all of the responses:

#### Response 1 ( $R_1$ ): Effect on vesicle size

$$\text{Vesicle size } (R_1) = +147.52 + 2.66 X_1 - 5.08 X_2 - 2.17 X_3 + 1.10 X_1 X_2 + 1.26 X_1 X_3 - 0.8575 X_2 X_3 + 23.47 X_1^2 + 13.40 X_2^2 - 5.09 X_3^2$$

It is important that the TN be of a tiny enough size to allow for increased cellular internalisation and cytosolic release of the medication that is entrapped within the cancer cells. According to what is shown in Table 2, the vesicle size of UA ranged from 145.5 nm to 192.58 nm, which indicates the development of TN with a small vesicle size. The above eq. of  $R_1$  and the various statistical plots that are displayed in Figure 1 demonstrate a substantial influence of all independent parameters on the vesicle size. There was a strong connection within the amount of Lipoid S100 present and the size of the vesicles found in the UA-TN. When the quantity of Lipoid S100 was taken from 60 mg to 100 mg, there was a discernible change in the size of the vesicles that contained TN. This change was attributable to a rise in the viscosity of the organic phase. During the process of the formation of UA-TN,

the increase viscosity of the lipid phase considerably reduces the shear efficiency, which is accountable for the drop in vesicle size.<sup>50</sup> The maximum viscosity of the organic part considerably decreases the diffusion rate from the organic to the aqueous part as a result of the Ostwald ripening phenomena, which further increases the vesicle size of the UA-TN.<sup>51</sup> A high interfacial tension can be advantageous to the coalescence of lipids, which can result in the synthesis of UA-TN with a larger vesicle size.<sup>52</sup> In a manner analogous, a slow rise in cholesterol from 10 to 20 mg progressively brings about a drop in the size of the vesicles that make up the UA-TN. However, increasing the dosage of the UA-TN from 15 mg to 25 mg causes the Span 60 to have a detrimental effect on the size of the vesicles produced by the UA-TN. Because of the decrease in the interfacial tension at the interface caused by an increase in Span 60 concentration, the vesicle size of the UA-TN considerably lowers as the concentration of Span 60 increases, which dramatically facilitates the emulsification of lipids inside the system. When it comes to the process that results in the formation of a vesicle, the concentration of the surfactant plays a major role.

#### Response 2 ( $R_2$ ): Effect on Entrapment Efficiency

$$\text{Entrapment efficiency } (R_2) = +83.69 + 5.53 X_1 + 2.17 X_2 - 1.23 X_3 - 0.5725 X_1 X_2 + 0.3600 X_1 X_3 - 0.2500 X_2 X_3 - 11.51 X_1^2 - 4.00 X_2^2 - 0.2042 X_3^2$$

One of the most significant benefits of growing TN is having a high percentage of EE. To reach the appropriate level of therapeutic effectiveness, the percentage of TN EE should be high. According to the findings as shown in Table 2, the percentage of EE in the formulation UA-TN ranges from 58.84% to 84.74%, which suggests the formulation of TN with appropriate loading capacity. In addition, the above eq. of  $R_2$  and the various statistical plots that are presented in Figure 1 demonstrate a considerable influence that is brought about by all of the independent components that are present. During the process of developing UA-TN, a progressive rise in the quantity of Lipoid S100 from 60 to 100 mg results in a large increase in the percentage of EE. Due to rise in the percentage of EE was attributable to an increase in the space for UA encapsulation in the hybrid matrix, which was achieved by increasing the amount of Lipoid S100, which supplies UA-TN with a much bigger percentage of EE.<sup>53</sup> When the amount of Span was taken from 15 to 25 mg, a comparable impact on %EE was observed. During the process of developing UA-TN, there was a gradual increase in the %EE, which may be attributed to a large increase in the viscosity of the organic phase brought about by an increase in the amount of lipoid S100. This resulted in quick solidification. The quick solidification of lipid considerably inhibits drug diffusion from the hybrid matrix, which results in TN with a larger percentage of effective energy.<sup>54</sup> The increased emulsification of Span 60 and Lipoid S100 inside the system during the creation of the formulation that gives the UA-TN a

high EE percentage can be linked to the fact that this increment in the %EE was measured. Despite this, there is a discernible drop in the percentage of electrons extracted from the UA-TN when the amount of cholesterol is taken from 10 to 20 mg. As encapsulated UA was portioned more from the internal to the external phase, its %EE decreased. Due to this, the hybrid matrix was able to leak less encapsulated drug, which resulted in UA-TN with low %EE.<sup>55</sup> It has been found that the hybrid matrix was responsible for the reduction in %EE. The hybrid matrix caused the encapsulated drug to be portioned more evenly between the internal and external phases, resulting in a lower %EE. As well as reducing the %EE of UA-TN, the hybrid matrix was found to contribute to the reduction.

### Response 3 (R<sub>3</sub>): Effect on *in vitro* release

$$\begin{aligned}
 \text{In vitro release (R}_3\text{)} = & +85.36 - 3.69 X_1 + 2.46 X_2 + 0.8037 \\
 & X_3 - 0.6525 X_1 X_2 - 1.30 X_1 X_3 + 0.3725 X_2 X_3 - 9.08 X_1^2 - 13.04 \\
 & X_2^2 - 7.95 X_3^2
 \end{aligned}$$

The vesicle size, which dramatically alters total therapeutic potential, is directly connected to the release of entrapped pharmaceuticals from the hybrid matrix of TN, which is a crucial parameter in obtaining the required therapeutic efficacy.<sup>56</sup> In order to achieve the required therapeutic efficacy, it is necessary to achieve the desired therapeutic efficacy. The nanoparticles with tiny vesicle sizes reflect the rapid release of encapsulated medicines Because of the large surface area.<sup>57</sup> On the other hand, nanoparticles with large vesicle sizes result in a relatively sluggish release of the encapsulated medication due to the reduced surface area available for diffusion.<sup>58</sup> According to the findings reported in Table 2, the *in vitro* release of UA-TN ranged from 58.84% to 86.28%, which suggests the creation of TN with regulated release properties. In addition, the polynomial equation of R3 and the various statistical graphs that are displayed in Figure 1 demonstrate a substantial influence of all independent parameters on *in vitro* drug release. The *in vitro* drug release of UA-TN is dramatically reduced when there is a gradual increase in the level of lipid

S100. The increase in viscosity that results in UA having a large vesicle size can be linked to the fact that there was a decrease in *in vitro* drug release when the Lipoid S100 concentration was increased.<sup>52</sup> The production of a thick and compact hybrid matrix of TN, which outcomes in fast drug diffusion, was ascribed to a considerable boost in the *in vitro* drug release on raising Span 60 concentration. This enhancement was due to the fact that the hybrid matrix was created. On the other hand, an increase in cholesterol amount was related with a rise in TN's drug release when tested *in vitro*. This augmentation in the *in vitro* drug release was ascribed to the synthesis of UA-TN with small vesicle size on account of an increase in cholesterol content.<sup>59</sup>

The improved formulation produced vesicles with a size of 145.5 ± 2.56 nm, a percentage entrapment efficiency of 84.74 ± 2.49%, an *in vitro* release of 86.28 ± 1.74% and zeta potential (Figure 2C). It was discovered that the value of the improved formulation was -12.22 mV. These results were shown in Figure 2. These values were quite close to the projected values that the Design-Expert programme had generated for particle size (153.70 nm), % EE (84.85%), and *in vitro* release (73.79%). Furthermore, the value of the PDI was found to be 0.172 after the formulation was improved. The improved formulation that was developed was then subjected to additional testing, which included vesicle morphology examination, CLSM and dermatokinetic investigation study.

### Morphology of UA-TN

The transmission electron micrograph of the improved UA-TN preparation demonstrated that the generated particles have a well identified sealed structure that is even in size distribution and spherical in shape (Figure 2B). The size of the particle, as determined by the Zeta sizer device by the use of the dynamic light scattering method, revealed a size distribution that was comparable to that which was presented in Figure 2A. The transmission electron micrograph showed that all of the ursolic acid was completely enclosed within the vesicular structure even though there were no drug crystals present.

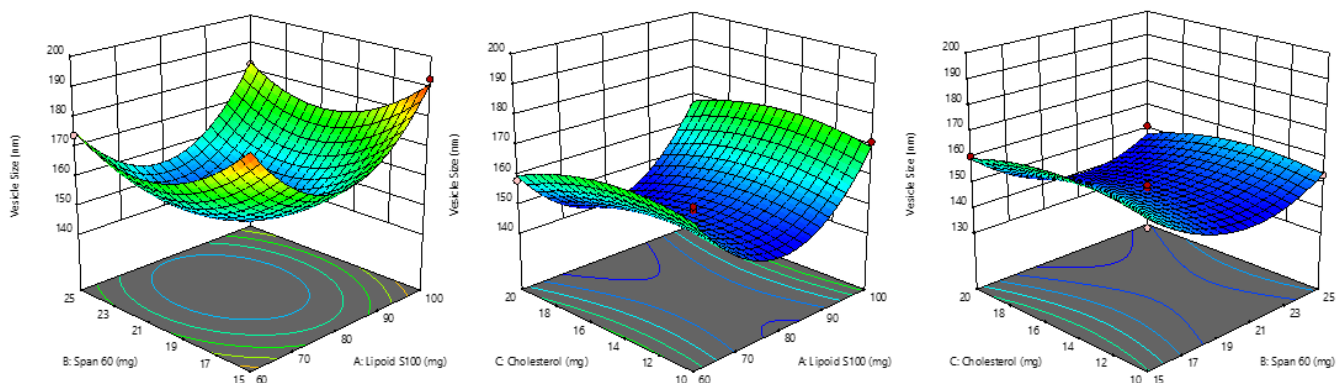


Figure 1: Representation of the 3D surface plot outcome of independent variables on (A) vesicle size, (B) EE and (C) *in vitro* drug release.

### %EE and %LC

For the preparation of the EE and LC to be effective, they need to be optimised in order to obtain the appropriate level of therapeutic efficacy. The UA-TN that was optimised showed an EE percentage of  $84.74 \pm 2.49\%$  and an LC percentage of  $8.29 \pm 0.36\%$ , respectively. Because of the hybrid matrix, the overall values of %EE and %LC for UA-TN were able to be optimised and found to be acceptable.

### In vitro release study

The release mechanism of the optimised UA-TN and UA-CF to ambient temperature with constant agitation at 100 rpm using the dialysis membrane process displayed a low percentage of drug released 40.91% from UA-CF as compared to optimised UA-TN, which presented maximum release up to 87.48%. This was due to the fact that optimised UA-TN was prepared using the dialysis bag method (Figure 3A). The results of the *in vitro* drug release testing were analysed by applying a variety of mathematical kinetics models to the data (zero-order, First order, Korsmeyer Peppas, Higuchi). When choosing an order for the release of

information, the correlation coefficient ( $R_2$ ) with the greatest value was given preference. In the instance of an optimised UA-TN, the Higuchi matrix model was found to have the greatest correlation coefficient value ( $R_2 = 0.8976$ ), followed by the first order model ( $R_2 = 0.8827$ ) and then the zero-order model ( $R_2 = 0.7139$ ). After optimising the UA-TN, Higuchi model was found the maximum possible value for the  $R^2$  that provided the greatest match.

By fitting the data into the Korsmeyer Peppas model, were able to analyse the release behaviour of UA from optimized UA-TN. Based on the regression analysis results, Determined the  $R^2$  level to be 0.9521 and the n value to be between 0 and 0.5 (0.2482). It appears to follow fickian diffusion when UA is released from optimised UA-TN.<sup>33</sup>

### Antioxidant activity

#### DPPH Assay

The antioxidant capacity of the UA-TN optimised formulation was compared to that of a reference material (ascorbic acid). Antioxidant activity was measured at 91.14% for the standard

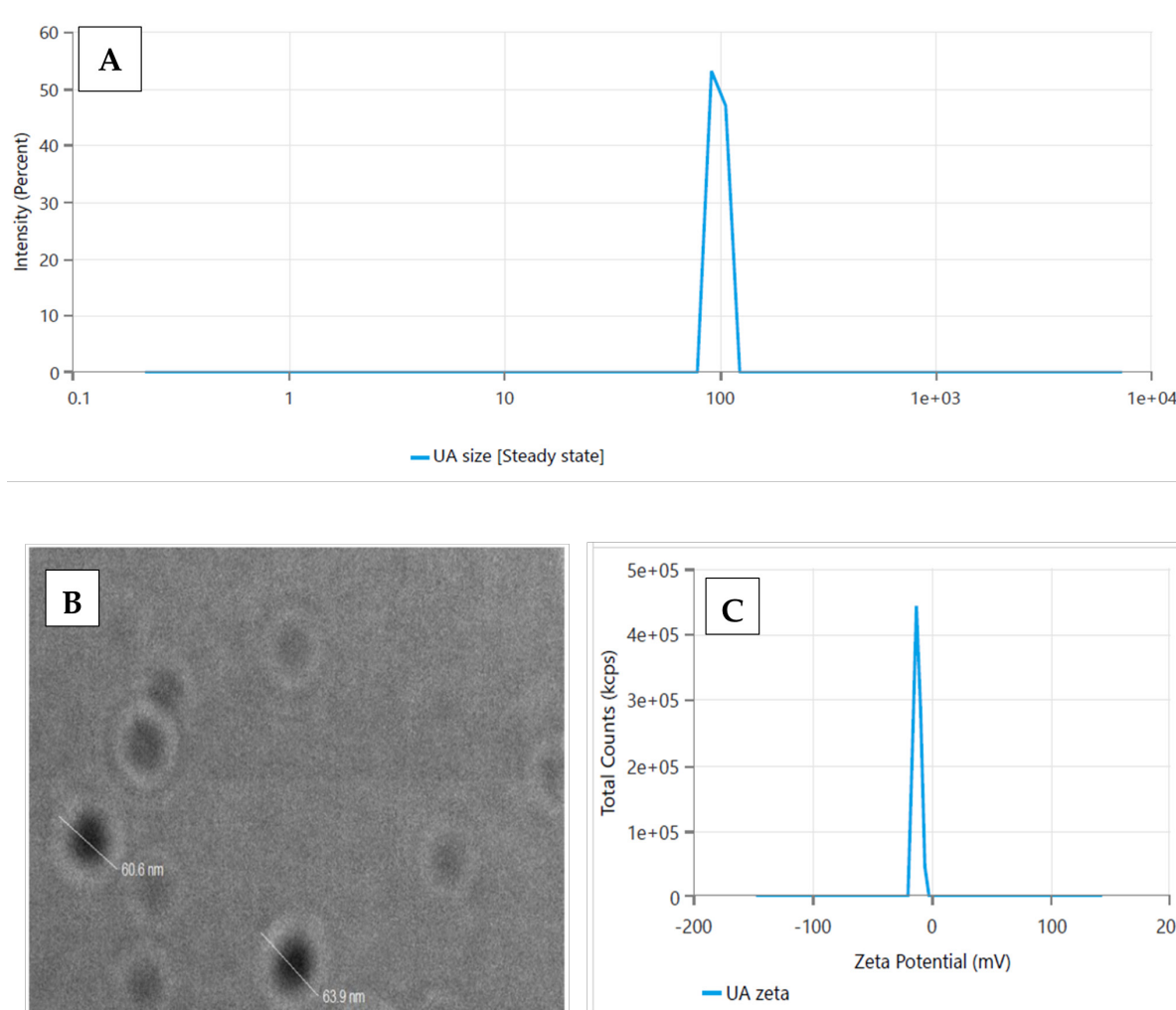


**Figure 2:** (A) Particles size using zeta sizer, (B) TEM, (C) Zeta Potential of optimized UA-TNs preparation.

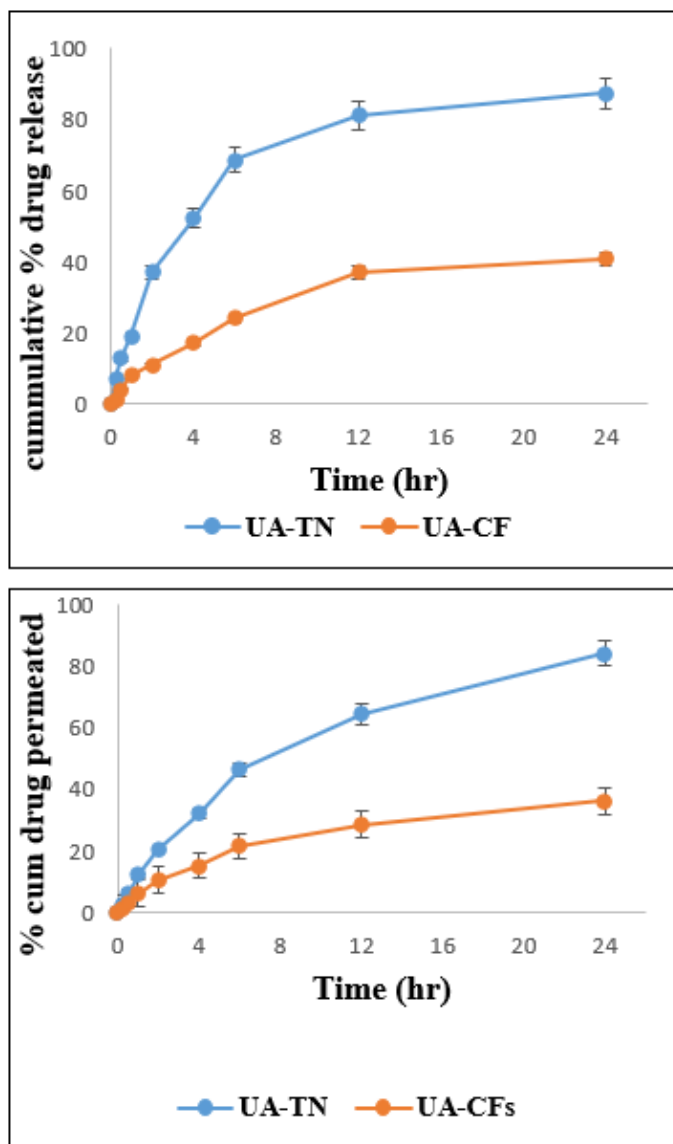


**Figure 3:** (A) *In vitro* drug release from UA-TN and UA suspension at pH 7.4. (B) *Ex vivo* graphs show cumulative amount of UA permeated through rat skin using UA-TN gel and UA-CF gel.

solution and 72.31% for the UA-TN optimised formulation, respectively. These findings provide further evidence that the UA-TN formulation possesses antioxidant properties. Even after the UA was encapsulated in the TN formulation, the antioxidant capacity of the UA was shown to be unaffected by this process, as indicated by the data that was collected.

**ABTS Assay**

The results of an ABTS experiment comparing the antioxidant profiles of UA and an improved version of UA-TN are displayed. According to the findings, both free UA and UA-TN showed concentration dependent %RSA in a manner that was comparable to that of the DPPH test. Both the optimised UA-TN and the free UA displayed %RSA values of 95.38% and 77.46%, respectively, when the concentration was set to 100 µg/mL. When compared with free UA, the optimised UA-TN demonstrated considerably increased (*p* < 0.05) %RSA activity. The boost in findings from improved UA-TN as a result of an improvement in the solubility of the encapsulated medication as well as the controlled diffusion of the drug from the hybrid nanoparticles.<sup>60</sup>

**Evaluation of optimized UA-TN gel Extrudability, Spreadability, Texture analysis and pH**

According to the results of the quality control test, gel formulations made using Carbopol 980 as the gelling agent were superior to other gel formulations that had both good extrudability and good spreadability.

pH of 6.8 was observed for the formulation of the UA-TN gel, which is very close to the skin pH. According to the reports that analysed the texture of the placebo gel, it had a firmness of 276.13g, a consistency of 1533.47g. sec, a cohesiveness of -226.09g, and an index of viscosity of -934.89g. sec. While the UA-TN gel had a 159.26g, 995.73g. sec, -134.37g, and -980.55g. sec are firmness, consistency, cohesiveness, index of viscosity respectively.

**Table 3: Dermatokinetic parameters of Ursolic Acid Conventional Preparation gel (UA-CF) and Ursolic Acid Transniosomes gel (UA-TN).**

Dermatokinetics Parameters	UA-CF gel		UA-TN gel	
	Epidermis	Dermis	Epidermis	Dermis
T <sub>skin max</sub> (h)	1.5 ± 0.1	2 ± 0.2	1.5 ± 0.1	2 ± 0.1
C <sub>skin max</sub> (µg/cm <sup>2</sup> )	53.03 ± 5.73	65.52 ± 3.50	146.85 ± 7.06	120.35 ± 6.74
AUC <sub>0-8</sub> (µg/cm <sup>2</sup> h)	241.35 ± 3.93	272.94 ± 20.6	660.18 ± 23.8	528.20 ± 23.7
Ke (h <sup>-1</sup> )	0.147 ± 0.11	0.120 ± 0.07	0.116 ± 0.10	0.07 ± 0.05

T<sub>skin max</sub> = Time to maximum concentration, C<sub>skin max</sub> = Maximum concentration, AUC = Area Under Curve, Ke = Elimination Rate Constant.

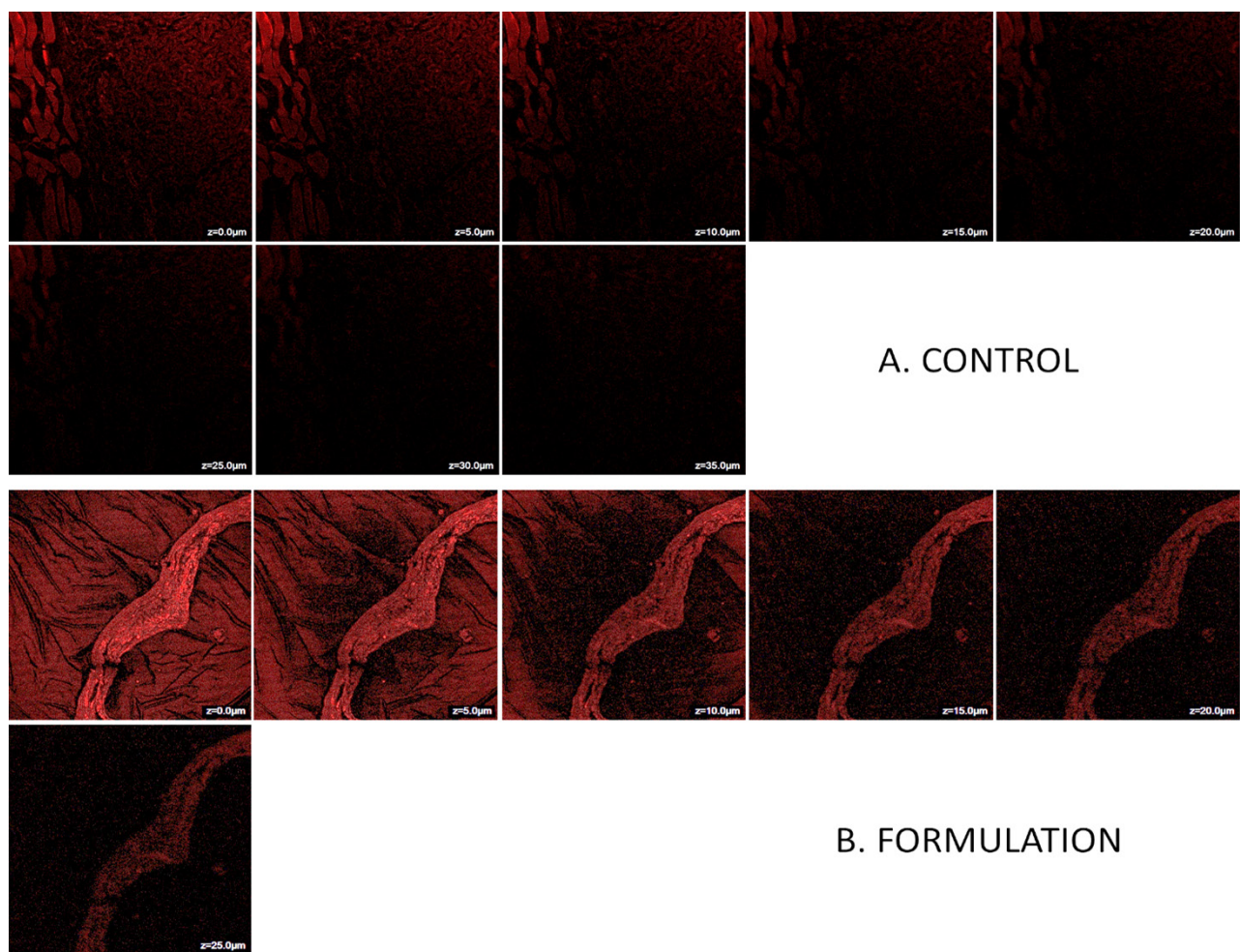


**Figure 4:** CLSM of (A) Rhodamine B solution and (B) Rhodamine B loaded Transniosomes showing a depth of penetration 10 μm and 25 μm across rat skin.

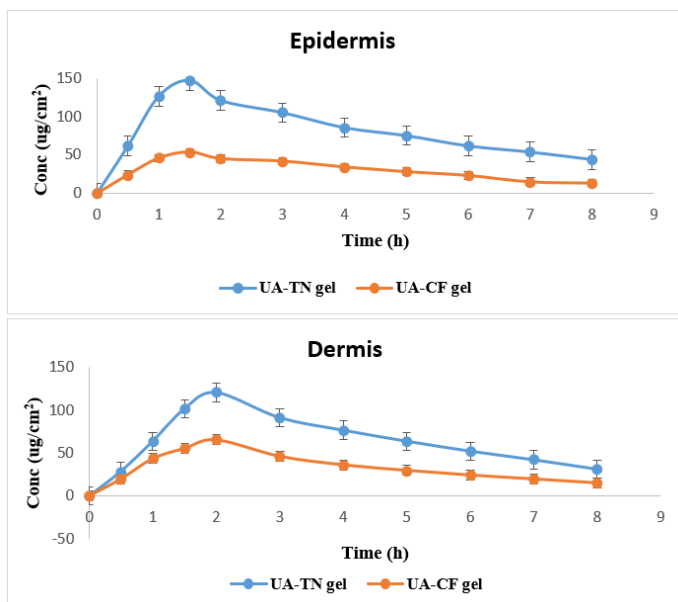


**Figure 5:** Shows UA quantity on (A) Epidermis and (B) dermis after topical application of UA-TN gel and UA-CF gel on excised rat skin.

### Skin permeation study of UA-TN gel

The release behaviour of the prepared optimised UA-TN gel and UA-CF gel was analysed using a Franz diffusion cell at ambient temperature with constant agitation at 600 RPM. The outcomes displayed that the UA-CF gel had a low percentage of cumulative drug permeated, which was 36.30%, in comparison to the UA-TN gel, which had a higher permeation of up to 84.05% (Figure 3B).

### Stability testing

Due to the fact that the F5 formulation that is 80 mg Lipoid S100, 20 mg Cholesterol and 15 mg Sodium Cholate (made with carbopol 934) displayed superior quality characteristics, a stability evaluation was done as per the requirements of the ICH. This was done so that the quality, safety, and efficacy of the drug could be maintained throughout its shelf life. There were no discernible shifts in the colour, odour, homogeneity, pH, or viscosity of the topical gel formulation after being subjected to stability tests for 0, 1, 2, 3 and 6 months. The outcomes of the investigation indicate that the topical gel F5 possesses a high degree of stability.

## Depth of skin penetration

According to the findings, a hydromethanolic solution of rhodamine B demonstrated a penetration of just 10  $\mu\text{m}$ , which indicates that it remained restricted to the skin's top layers exclusively (Figure 4A). On the other hand, rhodamine B-loaded TN gel went deeper, all the way up to 25  $\mu\text{m}$  (Figure 4B). The fact that the fluorescence is most intense in the intermediate layer of skin provides evidence that the formulation is kept in the epidermal layer below the surface. The maintenance of the formulation within the skin is essential for the treatment of a multitude of skin illnesses that are located in the lower epidermal area of the skin. As a result, it was possible to draw the conclusion that the TN gel that had been created was successful in delivering into the lower deposits of the mice's skin using rhodamine B dye.

## Dermatokinetic study

Figure 5 shows a representation of the relative concentration of UA in the dermis and epidermis of mice's skin following action with UA-CF gel and UA-TN gel at predefined time. The results of the statistical examination of the values are presented in Table 3. In comparison to the UA-CF gel, the skin that had been treated with UA-TN gel had considerably greater levels of  $C_{\text{Skin max}}$  and  $AUC_{0-8}$  throughout both layers (Table 3). It is possible that the capacity of vesicles to go through the skin's lipid layers is what is behind the extremely high retention rate of UA-TN gel. It was found that the  $T_{\text{Skin max}}$  of the UA-TN gel in the epidermis has a value that is equivalent to that of the UA-CF gel.

## CONCLUSION

In this study, the BBD was utilised for the purpose of optimising UA-TN formulations. The optimised UA-TN formulation demonstrated nanovesicle size as well as considerable entrapment efficiency together with a good *in vitro* release. The confocal analysis found that dye-laden hydro methanolic solution allowed for less penetration of rhodamine B loaded TN over the skin of mice than did rhodamine B loaded TN (control). Additional dermatokinetic research revealed that the UA-TN gel formulation had superior penetration versus the UA-CF gel formulation. Even after being incorporated into TN vesicles, the DPPH test confirmed that UA still has significant antioxidant activity. The current findings indicate that the TN formulation that was made is a potentially suitable drug carrier for the topical application of UA. Typically, TN vesicular systems will create depot in the lower skin layers and will constantly release the medicine over time. This is beneficial since it lowers the number of times that the medication will need to be applied.

## CONFLICT OF INTEREST

The authors declare that there is no conflict of interest.

## ABBREVIATIONS

**BBD:** Box-Behnken design; **CLSM:** Confocal laser scanning microscopy; **NF- $\kappa$ B:** Nuclear factor kappa B subunit; **NMSC:** Non-melanoma skin cancer; **PEG:** Polyethylene glycol; **STAT:** Signal transducer and activator of transcription; **TEM:** Transmission Electron Microscope; **TN:** Transniosomes; **TRAIL:** TNF-related apoptosis-inducing ligand; **UA:** Ursolic acid; **ZP:** Zeta potential.

## SUMMARY

The research aimed to optimize the preparation of Transniosomes (TN) for dermic distribution of Ursolic Acid (UA). The Box-Behnken design software was used to optimize the formulation, and evaluations were done on particle size, % EE, *in vitro* release, morphology, and dermatocokinetic studies. The optimal UA-TN formulation had sealed lamellae vesicles, particle size of  $145.5 \pm 2.56$  nm, % EE of  $84.74 \pm 2.49$ , and *in vitro* release of  $86.28 \pm 1.74\%$ . The confocal images of rat skin showed deeper penetration of the rhodamine B-loaded TN gel formulation, and the UA-TN gel applied to mouse skin had significant changes in  $C_{\text{Skin max}}$  and  $AUC_{0-8}$  compared to the UA-CF gel formulation. The research concluded that TN vesicle formulation was an effective drug carrier for UA topical delivery.

## REFERENCES

- Rogers HW, Weinstock MA, Feldman SR, Coldiron BM. Incidence estimate of nonmelanoma skin cancer (keratinocyte carcinomas) in the US population, 2012. *JAMA Dermatol.* 2015;151(10):1081-6. doi: 10.1001/jamadermatol.2015.1187, PMID 25928283.
- Doran CM, Ling R, Byrnes J, Crane M, Shakeshaft AP, Searles A, *et al.* Benefit cost analysis of three skin cancer public education mass-media campaigns implemented in New South Wales, Australia. *PLOS ONE.* 2016;11(1):e0147665. doi: 10.1371/journal.pone.0147665, PMID 26824695.
- Perera E, Gnaneswaran N, Staines C, Win AK, Sinclair R. Incidence and prevalence of non-melanoma skin cancer in Australia: A systematic review. *Australas J Dermatol.* 2015;56(4):258-67. doi: 10.1111/ajd.12282, PMID 25716064.
- Afaq F. Natural agents: cellular and molecular mechanisms of photoprotection. *Arch Biochem Biophys.* 2011;508(2):144-51. doi: 10.1016/j.abb.2010.12.007, PMID 21147060.
- Cohen JL. Actinic keratosis treatment as a key component of preventive strategies for nonmelanoma skin cancer. *J Clin Aesthet Dermatol.* 2010;3(6):39-44. PMID 20725550.
- Dzubak P, Hajduch M, Vydra D, Hustova A, Kvasnica M, Biedermann D, *et al.* Pharmacological activities of natural triterpenoids and their therapeutic implications. *Nat Prod Rep.* 2006;23(3):394-411. doi: 10.1039/b515312n, PMID 16741586.
- Hill RA, Connolly JD. Triterpenoids. *Nat Prod Rep.* 2013;29:780-818. doi: 10.1039/C3NP70032A.
- Sheng H, Sun H. Synthesis, biology and clinical significance of pentacyclic triterpenes: a multi-target approach to prevention and treatment of metabolic and vascular diseases. *Nat Prod Rep.* 2011;28(3):543-93. doi: 10.1039/c0np00059k, PMID 21290067.
- Shanmugam MK, Nguyen AH, Kumar AP, Tan BK, Sethi G. Targeted inhibition of tumor proliferation, survival, and metastasis by pentacyclic triterpenoids: potential role in prevention and therapy of cancer. *Cancer Lett.* 2012;320(2):158-70. doi: 10.1016/j.canlet.2012.02.037, PMID 22406826.
- Jinhua W. Ursolic acid: pharmacokinetics process *in vitro* and *in vivo*, a mini review. *Arch Pharm.* 2019;352(3):e1800222. doi: 10.1002/ardp.201800222, PMID 30663087.
- Eloy JO, Saraiva J, Albuquerque SD, Marchetti JM. Preparation, characterization and evaluation of the *in vivo* trypanocidal activity of ursolic acid-loaded solid dispersion with poloxamer 407 and sodium caprate. *Braz J Pharm Sci.* 2015;51:101-9. doi: 10.1590/S1984-82502015000100011.
- Saravanan R, Viswanathan P, Pugalendi KV. Protective effect of ursolic acid on ethanol-mediated experimental liver damage in rats. *Life Sci.* 2006;78(7):713-8. doi: 10.1016/j.lfs.2005.05.060, PMID 16137716.

13. Jin YR, Jin JL, Li CH, Piao XX, Jin NG. Ursolic acid enhances mouse liver regeneration after partial hepatectomy. *Pharm Biol.* 2012;50(4):523-8. doi: 10.3109/13880209.2011.611143, PMID 22136205.
14. Saaby L, Jäger AK, Moesby L, Hansen EW, Christensen SB. Isolation of immunomodulatory triterpene acids from a standardized rose hip powder (*Rosa canina* L.). *Phytother Res.* 2011;25(2):195-201. doi: 10.1002/ptr.3241, PMID 20632303.
15. Ali MS, Ibrahim SA, Jalil S, Choudhary MI. Ursolic acid: a potent inhibitor of superoxides produced in the cellular system. *Phytother Res.* 2007;21(6):558-61. doi: 10.1002/ptr.2108, PMID 17295383.
16. Zhang P, Cheng Y, Duan RD. Ursolic acid inhibits acid sphingomyelinase in intestinal cells. *Phytother Res.* 2013;27(2):173-8. doi: 10.1002/ptr.4709, PMID 22511398.
17. Pérez Gutiérrez RM, Vargas Solis R, Garcia Baez E, Gallardo Navarro YG. Hypoglycemic activity of constituents from *Astianthus viminalis* in normal and streptozotocin-induced diabetic mice. *J Nat Med.* 2009;63(4):393-401. doi: 10.1007/s11418-009-0343-7, PMID 19484331.
18. Do Nascimento PG, Lemos TL, Bizerra AM, Arriaga ÂM, Ferreira DA, Santiago GM, et al. Antibacterial and antioxidant activities of ursolic acid and derivatives. *Molecules.* 2014;19(1):1317-27. doi: 10.3390/molecules19011317, PMID 24451251.
19. Kurek A, Nadkowska P, Pliszka S, Wolska KI. Modulation of antibiotic resistance in bacterial pathogens by oleoanolic acid and ursolic acid. *Phytomedicine.* 2012;19(6):515-9. doi: 10.1016/j.phymed.2011.12.009, PMID 22341643.
20. Wu HY, Chang CI, Lin BW, Yu FL, Lin PY, Hsu JL, et al. Suppression of hepatitis B virus X protein-mediated tumorigenic effects by ursolic acid. *J Agric Food Chem.* 2011;59(5):1713-22. doi: 10.1021/jf1045624, PMID 21314126.
21. Kong L, Li S, Liao Q, Zhang Y, Sun R, Zhu X, et al. Oleoanolic acid and ursolic acid: novel hepatitis C virus antivirals that inhibit NS5B activity. *Antiviral Res.* 2013;98(1):44-53. doi: 10.1016/j.antiviral.2013.02.003, PMID 23422646.
22. Ishikawa T, Donatini R, Diaz IE, Yoshida M, Bacchi EM, Kato ET. Evaluation of gastroprotective activity of *Plinia edulis* (Vell.) *Sobral* (Myrtaceae) leaves in rats. *J Ethnopharmacol.* 2008;118(3):527-9. doi: 10.1016/j.jep.2008.05.007, PMID 18583075.
23. Shanmugam MK, Dai X, Kumar AP, Tan BK, Sethi G, Bishayee A. Ursolic acid in cancer prevention and treatment: molecular targets, pharmacokinetics and clinical studies. *Biochem Pharmacol.* 2013;85(11):1579-87. doi: 10.1016/j.bcp.2013.03.006, PMID 23499879.
24. Kuttan G, Pratheeshkumar P, Manu KA, Kuttan R. Inhibition of tumor progression by naturally occurring terpenoids. *Pharm Biol.* 2011;49(10):995-1007. doi: 10.3109/13880209.2011.559476, PMID 21936626.
25. Aggarwal BB, Shishodia S. Molecular targets of dietary agents for prevention and therapy of cancer. *Biochem Pharmacol.* 2006;71(10):1397-421. doi: 10.1016/j.bcp.2006.02.009, PMID 16563357.
26. Ovesná Z, Vachálková A, Horváthová K, Tóthová D. Pentacyclic triterpenoid acids: new chemoprotective compounds minireview. *Neoplasma.* 2004;51(5):327-33. PMID 15640935.
27. Shishodia S, Majumdar S, Banerjee S, Aggarwal BB. Ursolic acid inhibits nuclear factor- $\kappa$ B activation induced by carcinogenic agents through suppression of I $\kappa$ B $\alpha$  kinase and p65 phosphorylation: correlation with down-regulation of cyclooxygenase 2, matrix metalloproteinase 9, and cyclin D1. *Cancer Res.* 2003;63(15):4375-83. PMID 12907607.
28. Wang W, Zhao C, Jou D, Lü J, Zhang C, Lin LI, et al. Ursolic acid inhibits the growth of colon cancer-initiating cells by targeting STAT3. *Anticancer Res.* 2013;33(10):4279-84. PMID 24122993.
29. Pathak AK, Bhutani M, Nair AS, Ahn KS, Chakraborty A, Kadara H, et al. Ursolic acid inhibits STAT3 activation pathway leading to suppression of proliferation and chemosensitization of human multiple myeloma cells. *Mol Cancer Res.* 2007;5(9):943-55. doi: 10.1158/1541-7786.MCR-06-0348, PMID 17855663.
30. Prasad S, Yadav VR, Kannappan R, Aggarwal BB. Ursolic acid, a pentacyclic triterpene, potentiates TRAIL-induced apoptosis through p53-independent up-regulation of death receptors: evidence for the role of reactive oxygen species and JNK. *J Biol Chem.* 2011;286(7):5546-57. doi: 10.1074/jbc.M110.183699, PMID 21156789.
31. Wang J, Liu L, Qiu H, Zhang X, Guo W, Chen W, et al. Ursolic acid simultaneously targets multiple signaling pathways to suppress proliferation and induce apoptosis in colon cancer cells. *PLOS ONE.* 2013;8(5):e63872. doi: 10.1371/journal.pone.0063872, PMID 23737956.
32. Yin MC, Lin MC, Mong MC, Lin CY. Bioavailability, distribution, and antioxidative effects of selected triterpenes in mice. *J Agric Food Chem.* 2012;60(31):7697-701. doi: 10.1021/jf302529x, PMID 22816768.
33. Gupta DK, Aqil M, Ahad A, Imam SS, Waheed A, Qadir A, et al. Tailoring of berberine loaded transniosomes for the management of skin cancer in mice. *J Drug Deliv Sci Technol.* 2020;60:102051. doi: 10.1016/j.jddst.2020.102051.
34. Ahad A, Raish M, Ahmad A, Al-Jenoobi FI, Al-Mohizea AM. Development and biological evaluation of vesicles containing bile salt of telmisartan for the treatment of diabetic nephropathy. *Artif Cells Nanomed Biotechnol.* 2018;46(Sup 1):532-9. doi: 10.1080/21691401.2018.1430700, PMID 29373922.
35. Ahad A, Raish M, Ahmad A, Al-Jenoobi FI, Al-Mohizea AM. Eprosartan mesylate loaded bilosomes as potential nano-carriers against diabetic nephropathy in streptozotocin-induced diabetic rats. *Eur J Pharm Sci.* 2018;111:409-17. doi: 10.1016/j.ejps.2017.10.012, PMID 29030177.
36. Kazmi I, Al-Abbasi FA, Imam SS, Afzal M, Nadeem MS, Altayb HN, et al. Formulation and evaluation of apigenin-loaded hybrid nanoparticles. *Pharmaceutics.* 2022;14(4):783. doi: 10.3390/pharmaceutics14040783, PMID 35456617.
37. Xu XH, Su Q, Zang ZH. Simultaneous determination of oleoanolic acid and ursolic acid by RP-HPLC in the leaves of *Eriobotrya japonica* Lindl. *J Pharm Anal.* 2012;2(3):238-40. doi: 10.1016/j.jpaha.2012.01.006, PMID 29403748.
38. Khan S, Aamir MN, Madni A, Jan N, Khan A, Jabar A, et al. Lipid poly ( $\epsilon$ -caprolactone) hybrid nanoparticles for sustained release and enhanced anticancer efficacy. *Life Sci.* 2021;284:119909. doi: 10.1016/j.lfs.2021.119909, PMID 34450169.
39. Zafar A, Alruwaili NK, Imam SS, Alsaïdan OA, Ahmed MM, Yasir M, et al. Development and optimization of hybrid polymeric nanoparticles of apigenin: physicochemical characterization, antioxidant activity and cytotoxicity evaluation. *Sensors (Basel).* 2022;22(4):1364. doi: 10.3390/s22041364, PMID 35214260.
40. Pardeshi CV, Belgamwar VS, Tekade AR, Surana SJ. Novel surface modified polymer-lipid hybrid nanoparticles as intranasal carriers for ropinrole hydrochloride: *in vitro*, *ex vivo* and *in vivo* pharmacodynamic evaluation. *J Mater Sci Mater Med.* 2013;24(9):2101-15. doi: 10.1007/s10856-013-4965-7, PMID 23728521.
41. Ahad A, Aqil M, Kohli K, Sultana Y, Mujeeb M. The ameliorated longevity and pharmacokinetics of valsartan released from a gel system of ultra-deformable vesicles. *Artif Cells Nanomed Biotechnol.* 2016;44(6):1457-63. doi: 10.3109/21691401.2015.1041638, PMID 25953248.
42. Bhoopathy S, Inbakandan D, Rajendran T, Chandrasekaran K, Kasilingam R, Gopal D. Curcumin loaded chitosan nanoparticles fortify shrimp feed pellets with enhanced antioxidant activity. *Mater Sci Eng C Mater Biol Appl.* 2021;120:111737. doi: 10.1016/j.msec.2020.111737, PMID 33545880.
43. Pauluk D, Padilha AK, Khalil NM, Mainardes RM. Chitosan-coated zein nanoparticles for oral delivery of resveratrol: formation, characterization, stability, mucoadhesive properties and antioxidant activity. *Food Hydrocoll.* 2019;94:411-7. doi: 10.1016/j.foodhyd.2019.03.042.
44. Ahad A, Aqil M, Ali A. Investigation of antihypertensive activity of Carbopol valsartan transdermal gel containing 1, 8-cineole. *Int J Biol Macromol.* 2014;64:144-9. doi: 10.1016/j.ijbiomac.2013.11.018, PMID 24296403.
45. Ahad A, Aqil M, Kohli K, Sultana Y, Mujeeb M. Design, formulation and optimization of valsartan transdermal gel containing iso-eucalyptol as novel permeation enhancer: preclinical assessment of pharmacokinetics in Wistar albino rats. *Expert Opin Drug Deliv.* 2014;11(8):1149-62. doi: 10.1517/17425247.2014.914027, PMID 24830648.
46. Moolakkadath T, Aqil M, Ahad A, Imam SS, Praveen A, Sultana Y, et al. Preparation, and optimization of fisetin loaded glycerol based soft nanovesicles by Box-Behnken design. *Int J Pharm.* 2020;578:119125. doi: 10.1016/j.ijpharm.2020.119125, PMID 32036010.
47. Aiyalu R, Govindarjan A, Ramasamy A. Formulation and evaluation of topical herbal gel for the treatment of arthritis in animal model. *Braz J Pharm Sci.* 2016;52(3):493-507. doi: 10.1590/S1984-82502016000300015.
48. Negi P, Singh B, Sharma G, Beg S, Katare OP. Biocompatible lidocaine and prilocaine loaded-nanoemulsion system for enhanced percutaneous absorption: QbD-based optimisation, dermatokinetics and *in vivo* evaluation. *J Microencapsul.* 2015;32(5):419-31. doi: 10.3109/02652048.2015.1046513, PMID 26066775.
49. Chaudhari A, Mashru R. Development, and validation of analytical method of berberine and its quantification in multicomponent homeopathic formulations. *World J Pharm Res.* 2017;6:793-802. doi: 10.20959/wjpr20175-8337.
50. Tahir N, Madni A, Balasubramanian V, Rehman M, Correia A, Kashif PM, et al. Development and optimization of methotrexate-loaded lipid-polymer hybrid nanoparticles for controlled drug delivery applications. *Int J Pharm.* 2017;533(1):156-68. doi: 10.1016/j.ijpharm.2017.09.061, PMID 28963013.
51. Ravi PR, Vats R, Dalal V, Gaddekar N, N A. Design, optimization and evaluation of poly- $\epsilon$ -caprolactone (PCL) based polymeric nanoparticles for oral delivery of lopinavir. *Drug Dev Ind Pharm.* 2015;41(1):131-40. doi: 10.3109/03639045.2013.850710, PMID 24180260.
52. Thakur K, Sharma G, Singh B, Chhibber S, Patil AB, Katare OP. Chitosan-tailored lipidic nanoconstructs of fusidic acid as promising vehicle for wound infections: an explorative study. *Int J Biol Macromol.* 2018;115:1012-25. doi: 10.1016/j.ijbiomac.2018.04.092, PMID 29680503.
53. Gajra B, Dalwadi C, Patel R. Formulation and optimization of itraconazole polymeric lipid hybrid nanoparticles (Lipomer) using box Behnken design. *Daru J Pharm.* 2015;23:1-5. doi: 10.1186%2F40199-014-0087-0.
54. Asfour MH, Salama AAA, Mohsen AM. Fabrication of all-trans retinoic acid loaded chitosan/tripolyphosphate lipid hybrid nanoparticles as a novel oral delivery approach for management of diabetic nephropathy in rats. *J Pharm Sci.* 2021;110(9):3208-20. doi: 10.1016/j.xphs.2021.05.007, PMID 34015278.
55. Leonardi A, Bucolo C, Romano GL, Platania CB, Drago F, Puglisi G, et al. Influence of different surfactants on the technological properties and *in vivo* ocular tolerability of lipid nanoparticles. *Int J Pharm.* 2014;470(1-2):133-40. doi: 10.1016/j.ijpharm.2014.04.061, PMID 24792979.

56. Blanco E, Shen H, Ferrari M. Principles of nanoparticle design for overcoming biological barriers to drug delivery. *Nat Biotechnol.* 2015;33(9):941-51. doi: 10.1038/nbt.3330, PMID 26348965.
57. Tibbitt MW, Dahlman JE, Langer R. Emerging frontiers in drug delivery. *J Am Chem Soc.* 2016;138(3):704-17. doi: 10.1021/jacs.5b09974, PMID 26741786.
58. Shahab MS, Rizwanullah M, Alshehri S, Imam SS. Optimization to development of chitosan decorated polycaprolactone nanoparticles for improved ocular delivery of dorzolamide: *in vitro*, *ex vivo* and toxicity assessments. *Int J Biol Macromol.* 2020;163:2392-404. doi: 10.1016/j.ijbiomac.2020.09.185, PMID 32979440.
59. Garg NK, Singh B, Sharma G, Kushwah V, Tyagi RK, Jain S, *et al.* Development and characterization of single step self-assembled lipid polymer hybrid nanoparticles for effective delivery of methotrexate. *RSC Adv.* 2015;5(77):62989-99. doi: 10.1039/C5RA12459J.
60. Zhang J, Wang D, Wu Y, Li W, Hu Y, Zhao G, *et al.* Lipid-polymer hybrid nanoparticles for oral delivery of Tartary buckwheat flavonoids. *J Agric Food Chem.* 2018;66(19):4923-32. doi: 10.1021/acs.jafc.8b00714, PMID 29696978.

**Cite this article:** Makeen HA, Bratty MA. Ursolic Acid Loaded Transniosomes Nanogel for Topical Delivery: Statistical Optimization with Box-Behnken Design of Quality by Design (QbD), *in vitro* and Dermatokinetic Evaluation. *Indian J of Pharmaceutical Education and Research.* 2024;58(1):109-21.